Modulated optical structures over a modulationally stable medium

Céline Durniak and Majid Taki*
Laboratoire de Physique des Lasers, Atomes et Molécules, UMR CNRS 8523, Université des Sciences et Technologies de Lille, F-59655 Villeneuve d'Ascq, France

Mustapha Tlidi†
Optique Nonlinéaire Théorique, Université Libre de Bruxelles, Code Postal 231, B-1050 Bruxelles, Belgium

Pier Luigi Ramazza and Umberto Bortolozzo
Istituto Nazionale di Ottica Applicata, I50125 Florence, Italy

Gregory Kozyreff
Oxford Centre for Industrial and Applied Mathematics, Oxford University, Oxford OX1 3LB, United Kingdom
(Received 18 October 2004; revised manuscript received 8 June 2005; published 17 August 2005)

Evidence of modulated dissipative structures with an intrinsic wavelength in a nonlinear optical system devoid of Turing instability is given. They are found in the transverse field distribution of an optical cavity containing a liquid crystal light valve. Their existence is related to a transition from flat to modulated fronts connecting the unstable middle branch of a bistability cycle and either of the two stable uniform states. We first analyze the cavity in the limit of nascent bistability, where a modified Swift-Hohenberg equation is derived. This allows for a simple analytical expression of the threshold associated with the transition as well as the wavelength of the emerging structure. Numerical simulations show development of ring-shaped modulated fronts and confirm analytical predictions. We then turn to the full model and find the same transition, both analytically and numerically, proving that this transition in not limited to nascent bistability regimes.

DOI: 10.1103/PhysRevE.72.026607 PACS number(s): 42.65.Sf, 05.40.Ca, 05.45.−a

I. INTRODUCTION

Pattern formation in extended systems has attracted much attention in fields as different as physics, hydrodynamics, chemistry, and biology [1]. Nonlinear optics, in particular, represents a fruitful area of activity [2,3]. This is due to the fact that patterned states arise naturally in many optical devices from the interplay of diffraction, nonlinearities and dissipation. Among the nonlinear systems analyzed, the optical devices formed by a thin slice of nonlinear material with feedback [4] are the subject of intense research, both theoretical and experimental, owing to their ability to exhibit a rich variety of ordered or complex structures, including regular patterns [5], space-time chaotic dynamics [6], and dissipative solitons [7]. Experimental realizations of this scheme are typically based on liquid crystal cells or the liquid crystal light valve (LCLV) as nonlinear media. Recent investigations in these experimental systems have focused on localized structures [8] and the occurrence of noise-sustained structures in the presence of drift transport [9]. More recently, bistability between round and triangular localized structures has been demonstrated experimentally in this system [10].

The purpose of this article is to report on the occurrence of modulated structures with an intrinsic wavelength in a modulationally stable regime, i.e., in a regime far from any modulational instability (Turing instability, [11]). These modulations spontaneously develop from *localized* perturbations of the *unstable* homogeneous steady state that separates the two stable states of a hysteresis cycle. This constitutes the counterpart of Turing spontaneous modulations initiated by *extended* perturbations. They occur in the wings of the traveling fronts and eventually give rise to a self-organized propagating pattern. The analytical expressions of their wavelengths and velocities are explicitly derived. Such non-Turing structures have been predicted in some one-dimensional models in fluid mechanics [12]. But, as far as we are aware, they have never been observed in any experimental system. In this paper, we analyze the LCLV nonlinear optical cavity as a candidate for this purpose.

Note that different types of non-Turing modulations have been reported in optical bistability [13], and in the degenerate optical parametric oscillator with walk-off [14]. In the former case, the modulation results from the tail interaction between switching waves (see also the book by Rosanov on this subject, [3]). In the latter case, the modulated structures are directly produced by walk-off; without it, they do not exist, at least in the range of parameters considered in [14]. By contrast, in the dynamical regime considered here, no walk-off nor any form of preexisting drift is necessary to generate the pattern. In particular, the modulations are characterized by an intrinsic wavelength which is determined solely by dynamical parameters and not by convection. In addition, we establish their existence in the parameter space, and observe a transition from flat to two-dimensional modulated non-Turing structures in the form of ring-shaped fronts.

The remainder of the paper is organized as follows. In Sec. II, we recall the model describing a LCLV cavity and

*Electronic address: taki@phlam.univ-lille1.fr
†Electronic address: mtlidi@ulb.ac.be

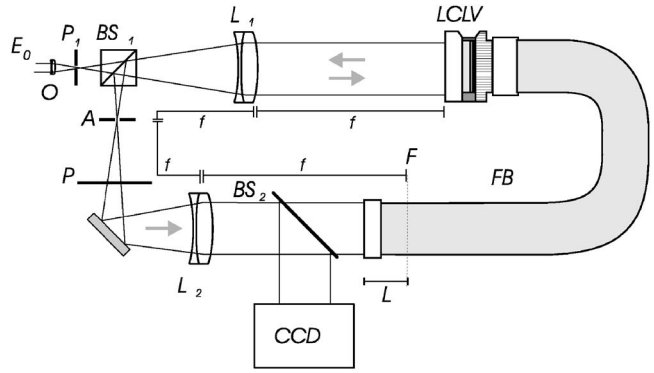

FIG. 1. Typical experimental setup. E_0, input field ($I_0=|E_0|^2$); O, microscope objective; P_1,A, pinholes; BS_1,BS_2, beam splitters; LCLV, liquid crystal light valve; L_j, lenses, all with focal length f; P, polarizer; CCD, charge-coupled device video camera; the feedback is achieved through the fiber bundle FB.

derive the modified Swift-Hohenberg equation in the limit of nascent bistability. We exploit this simplification in Sec. III, where we investigate in detail the origin of structuring in the system, namely the appearance of modulations in the front connecting an unstable homogeneous steady state to another stable one. In Sec. IV, we return to the full model and study the transition between flat and modulated front without any approximation. Finally, we summarize and conclude.

II. FULL AND SIMPLIFIED MODELS

The system we consider is a cavity whose nonlinear active element is a LCLV. Figure 1 depicts a typical experimental setup. The main control parameters are the injected field E_0, the polarizer P, and the rms voltage V_0 applied across the LCLV. A certain fraction of V_0 applies to the nematic liquid crystals cell inside the LCLV and reorients them. This reorientation induces a phase retardation on the electromagnetic wave going through the cell. In first approximation, the phase retardation is proportional to the impinging intensity and thus causes a Kerr effect. The dynamics of the electromagnetic field inside the cavity is thus described by the optical phase ϕ retardation in the LCLV. Normalizing the time and space variables by the response time and diffusion length of the LCLV, ϕ satisfies [15]

$$\frac{\partial \phi}{\partial \tau} = \phi_0 - \phi + \nabla^2 \phi + f(I_{fb}), \tag{1}$$

where $\phi_0=\phi_0(V_0)$ is a constant phase retardation due to the voltage applied to the cell, ∇^2 is the Laplacian acting on the transverse coordinates $\mathbf{x}=(x_1,x_2)$, and $f(I_{fb})$ is the nonlinear response to the feedback field intensity I_{fb}.

We shall assume a Kerr-type response with coefficient α and saturation φ_{sat}, so that

$$f(I_{fb}) = \varphi_{sat}(1 - e^{-\alpha I_{fb}/\varphi_{sat}}) \approx \alpha I_{fb} - (\alpha I_{fb})^2/2\varphi_{sat}.$$

As explained in [15], for an injected intensity $I_0=|E_0|^2$, the feedback intensity is given by

$$I_{fb} = I_0 |e^{-ia\nabla^2}(Me^{-i\phi} + N)|^2,$$

where $|M|=\cos^2\theta$, $|N|=\sin^2\theta$, and $a=cL/(2\omega\ell^2)$. The expression for I_{fb} arises from the formal resolution of the free-space propagation problem in the cavity feedback loop. The amplitudes M and N are relative to the field components polarized along the LC director and perpendicular to it, respectively. These two components are projected, via a polarizer, on a common direction θ with respect to the LC director. In the expression for a, L is the free propagation length, c is the speed of light, ω is the frequency of the electromagnetic wave, and ℓ is the phase diffusion length in the LCLV. The parameter a is the normalized diffraction coefficient, which can be controlled through ω and L.

The expression for I_{fb} greatly complicates the study of Eq. (1). Fortunately, one can simplify this equation while retaining the dynamics we wish to describe by considering this equation near the limit of nascent bistability and assuming, for the sake of simplicity, $\theta \approx \pi/4$. This last assumption is by no means necessary but simplifies notably the algebra arising from trigonometric nonlinearties. We shall follow the same methodology as that recently described in [16] and, previously, in [17].

We first recall that the homogeneous solutions of Eq. (1) are given by

$$\begin{aligned} 0 &= \phi_0 - \phi - \varphi_{sat}\{1 - \exp[\alpha I_0 \cos^2(\phi/2)/\varphi_{sat}]\} \\ &= \phi_0 - F(\phi, \alpha I_0, \theta) \end{aligned} \tag{2}$$

and that linear perturbations $\propto \exp(ikx+\lambda\tau)$ obey the dispersion relation

$$\lambda = -(1+k^2) - \alpha I_0 e^{-\alpha I_{fb}/\varphi_{sat}} \cos\left(\frac{\phi}{2}\right) \sin\left(\frac{\phi}{2} - ak^2\right). \tag{3}$$

The input-output characteristic will be close to bistability regime when $\partial F/\partial\phi, \partial^2 F/\partial\phi^2 \approx 0$. These two conditions yield the critical values $\phi=\phi_c$ and $\alpha I_0=\alpha I_c$, such that

$$\alpha I_c \sin\phi_c[(1+\cos\phi_c)\alpha I_c - 2\varphi_{sat}] - 4\varphi_{sat} = 0$$

and

$$\left(1 + \frac{\cos 2\phi_c}{\cos\phi_c}\right)\alpha I_c - 2\varphi_{sat} = 0.$$

If we particularize the linear stability analysis to $\phi=\phi_c$, $\alpha I_0=\alpha I_c$ and to small wave numbers $k \ll 1$, Eq. (3) simplifies into

$$\lambda \sim -k^2\left[1 + a\cot\left(\frac{\phi_c}{2}\right) + a^2k^2/2 + \cdots\right]. \tag{4}$$

The k^2 factor above means that homogeneous perturbations are marginally stable. This results from the coalescence of two limit points at $\phi=\phi_c$. In addition, Eq. (4) clearly indicates the possibility of a nontrivial dynamics at small but finite k's if the diffraction parameter a is close to

$$a_c = -\tan\left(\frac{\phi_c}{2}\right).$$

For a typical value $\varphi_{sat}=5$, we find $\alpha I_c=2.55$, $\phi_c=4.42$, and $a_c=1.35$.

Let us now introduce a small parameter ε and the expansions

$$\phi = \phi_c + \varepsilon\psi(\boldsymbol{\xi},t), \quad \alpha I_0 = \alpha I_c + \varepsilon^2 \alpha I_2,$$

$$\theta = \frac{\pi}{4} + \varepsilon\theta_1, \quad \phi_0 = F(\phi_c, \alpha I_0, \theta) + \varepsilon^3\psi_0,$$

$$a = a_c + \varepsilon a_1, \quad \boldsymbol{\xi} = (\varepsilon/a_c)^{1/2}\mathbf{x}, \quad t = \varepsilon^2\tau.$$

A simple substitution in Eq. (1) yields, after lengthy calculations, the following amplitude equation:

$$\frac{\partial\psi}{\partial t} = \psi_0 + B\psi - C\psi^3 + \mathcal{D}(\psi)\nabla^2\psi - |\nabla\psi|^2 - \frac{1}{2}\nabla^4\psi, \quad (5)$$

where ∇ now means $(\partial/\partial\xi_1, \partial/\partial\xi_2)$ and $\mathcal{D}(\psi)=D-E\psi$ is a nonlinear diffusion coefficient. The quantities B, C, D, and E are related to all physical parameters defined in Eq. (1) through

$$B = \frac{\sin\phi_c}{2\varphi_{sat}}\{[(1+\cos\phi_c)\alpha I_c - \varphi_{sat}]\alpha I_2 + 4\alpha I_c(\varphi_{sat} - \alpha I_c\cos\phi_c)\theta_1^2\},$$

$$C = \frac{\alpha I_c \sin\phi_c}{24\varphi_{sat}}[(1+4\cos\phi_c)\alpha I_c - 2\varphi_{sat}],$$

$$D = \frac{\alpha I_c}{4a_c\varphi_{sat}}[(1+\cos\phi_c)\alpha I_c - 2\varphi_{sat}] \times [(1+\cos\phi_c)a_1 - 4a_c\theta_1],$$

$$E = \frac{\alpha I_c \sin\phi_c}{2\varphi_{sat}}[(1+\cos\phi_c)\alpha I_c - \varphi_{sat}].$$

For $\varphi_{sat}=5$, we have

$$B = 0.3\alpha I_2 - 5.6\theta_1^2, \quad C = 0.21,$$

$$D = 4.17\theta_1 - 0.55a_1, \quad E = 0.77.$$

Note that Eq. (5) has been first introduced in the context of semiconductor laser dynamics [16], and later derived independently by us and in [18] for the LCLV close to nascent bistability. It resembles the well-known Swift-Hohenberg equation but the nonlinear diffusive term breaks the reflection invariance $\psi \leftrightarrow -\psi$.

III. THE MODIFIED SWIFT-HOHENBERG EQUATION

The homogeneous steady states (HSSs) of Eq. (5) are implicitly given by

$$\psi_0 = C\psi_s^3 - B\psi_s.$$

The coefficient C is always positive and, in what follows, we assume $B>0$ in order to ensure that the system is bistable.

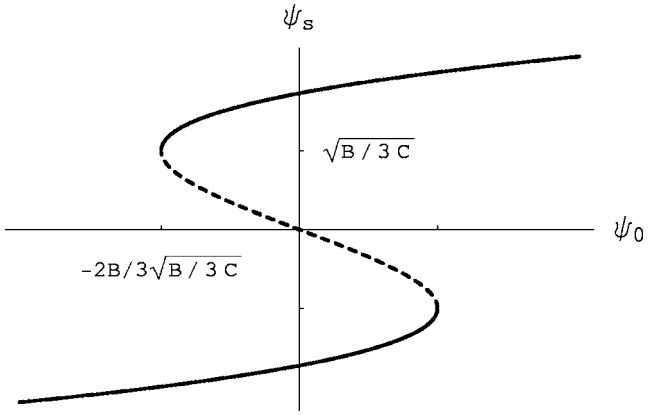

FIG. 2. Bistability cycle in the modified Swift-Hohenberg equation, when $B>0$.

The unstable branch connecting the two stable states of the hysteresis cycle extends from $\psi_s=-\sqrt{B/3C}$ to $\psi_s=\sqrt{B/3C}$ and is illustrated in Fig. 2. Let us now analyze the linear stability of the HSSs with respect to perturbations of the form $\psi=\psi_s+\delta\exp(\lambda t+i\mathbf{k}\cdot\boldsymbol{\xi})$ where $\mathbf{k}$ is the (real) wave vector of the perturbation and λ its growth rate. Keeping only linear contributions in δ, we soon find that λ and $\mathbf{k}$ must satisfy

$$\lambda = -\frac{d\psi_0}{d\psi_s} - \mathcal{D}(\psi_s)k^2 - \frac{1}{2}k^4, \quad (6)$$

where

$$\frac{d\psi_0}{d\psi_s} = -B + 3C\psi_S^2$$

and k^2 stands for the square modulus of $\mathbf{k}$. A Turing instability occurs when $\lambda=0$ and $d\lambda/dk=0$ for a finite and real k. One can easily show that this does not occur for any steady state ψ_s provided that

$$D > E\sqrt{B/3C}.$$

In the sequel we focus on this range of parameters. Since the system is stable to Hopf and Turing bifurcations, no extended modulation, either in space or time, can grow in the system. However, Fig. 3 shows that localized disturbances from the unstable branch $-\sqrt{B/3C}<\psi_s<\sqrt{B/3C}$ can in fact display oscillations. In the numerical simulations, the perturbation is initiated in the form of a radially symmetric impulsion, as could physically be caused by a laser beam. For sufficiently large values of B, the front leaves a spatial modulation behind its passage, so that, eventually, the entire domain is covered by a spatially modulated solution.

The classical linear stability theory is insufficient, as it stands, to explain the above observations because it applies to extended perturbations characterized by a single wave number. By contrast, in order to determine the linear response of the system to a localized perturbation, it is necessary to include a finite band of modes in the dynamical description. This can be achieved by reformulating the linear stability analysis as an initial-value problem. For a detailed description of the concept and techniques of instabilities in

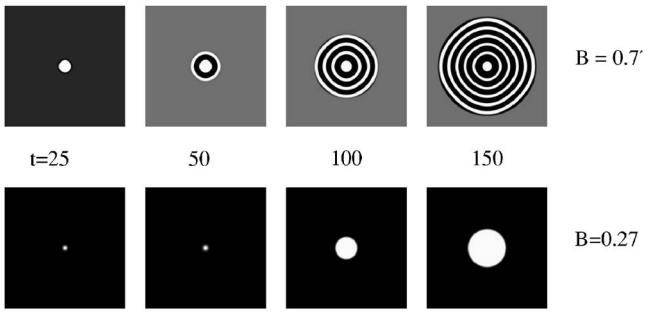

FIG. 3. Transition from flat to two-dimensional non-Turing modulated dissipative structures obtained numerically from the model Eq. (5). The parameters are $E=0.77$, $C=1.5$. $D=1$, and $\psi_0=0.04$.

terms of an initial-value problem analysis (including absolute and convective instabilities), the reader is referred to the original work by Briggs [19], or the new formulations by Brevdo [20], and the recent works in optics [14,21,22].

In one spatial direction, let us consider the evolution of $\psi=\psi_s+\delta A(\xi,t)$, where, initially,

$$A(\xi,0)=\int_{-\infty}^{\infty}\bar{A}(k)e^{ik\xi}dk.$$

From Eq. (6), at later times we have

$$A(\xi,t)=\int_{-\infty}^{\infty}\bar{A}(k)e^{t\Delta(k)}dk, \tag{7}$$

where $\Delta(k)=\lambda(k)+ik\xi/t$ and we need to evaluate this integral asymptotically as $t\to\infty$, with $\xi/t\equiv V=O(1)$.

Following the method of steepest descent [23], we deform the path of integration in Eq. (7) in the complex plane $k=k_r+ik_i$ and look for the complex wave number $k_c=k_{r,c}+ik_{i,c}$, such that $(\partial/\partial k_r)\mathrm{Re}[\Delta(k_r,k_i)]=(\partial/\partial k_i)\mathrm{Re}[\Delta(k_r,k_i)]=0$. We then use the result that, asymptotically,

$$A(\xi,t)\propto e^{t\Delta(k_c)}=e^{\xi\Delta(k_c)/V}. \tag{8}$$

Finally, the front is the part of the perturbation that travels into the unstable region without changing amplitude. Hence, we require that $\mathrm{Re}[\Delta(k_r,k_i)]=0$. This happens when the group velocity is identical to the envelope velocity of the front [12]. These three conditions on $\mathrm{Re}[\Delta(k_r,k_i)]$ determine k_r, k_i, and $V=\xi/t$ as a function of ψ_s. The value of k_r characterizes the spatial modulation of the front, k_i determines its spatial decay, and V its speed.

We find that both modulated ($k_r\neq 0$) and flat ($k_r=0$) fronts are indeed possible. We have characterized the parameter range for each one of the two dynamical behaviors. We find that the formation of propagating patterns is possible only if

$$\mathcal{D}(\psi_s)^2\leqslant -6\frac{d\psi_0}{d\psi_s}, \tag{9}$$

where we recall that ψ_s is on the unstable middle branch of the bistability cycle. The modulated front characteristics are then given by

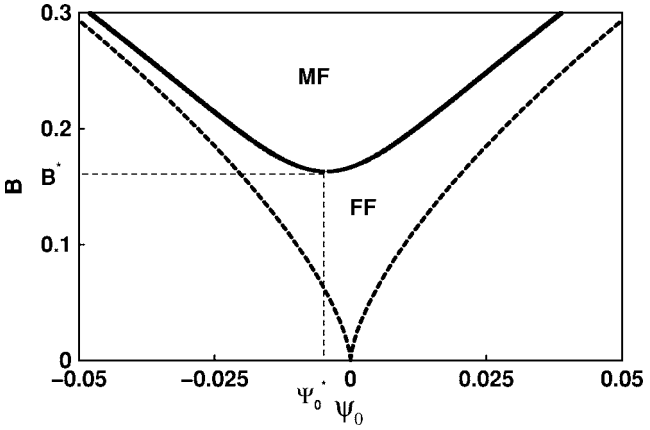

FIG. 4. Transition from flat to modulated fronts in the modified Swift-Hohenberg model in the (ψ_0,B) plane. MF, modulated fronts; FF, flat fronts. Dashed lines delimit the region of existence of the unstable homogeneous steady state. The parameters are the same as in Fig. 3.

$$k_r^2=(1/4)=\left[-3\mathcal{D}(\psi_s)+\sqrt{7\mathcal{D}(\psi_s)^2-12\frac{d\psi_0}{d\psi_s}}\right], \tag{10}$$

$$k_i^2=(1/3)[\mathcal{D}(\psi_s)+k_r^2], \tag{11}$$

$$V_{MF}=(4\sqrt{3}/9)[\mathcal{D}(\psi_s)+4k_r^2]\sqrt{\mathcal{D}(\psi_s)+k_r^2}. \tag{12}$$

On the other hand, flat fronts occur when $\mathcal{D}(\psi_s)^2\geqslant -6(d\psi_0/d\psi_s)$, and propagate with a velocity $V_{FF}=2k_i[\mathcal{D}(\psi_s)+k_i^2]$ where

$$k_i^2=(1/3)\left[\mathcal{D}(\psi_s)-\sqrt{\mathcal{D}(\psi_s)^2+6\frac{d\psi_0}{d\psi_s}}\right]. \tag{13}$$

In two spatial dimensions, the complex wave number becomes a complex wave vector $\mathbf{k}=(k_{1r}+ik_{1i},k_{2r}+ik_{2i})$. After a lengthy calculation, we find that a calculation of the same kind as above leads to the same formulas (5)–(9) but where k_r and k_i are replaced by $\sqrt{k_{1r}^2+k_{2r}^2}$ and $\sqrt{k_{1i}^2+k_{2i}^2}$. The above results are summarized in the bifurcation diagram of Figs. 4 and 5. Figure 4 shows the transition between flat fronts (FF) and modulated fronts (MF) in the (ψ_0,B) plane, as given by the limiting curve of expression (9). The transition threshold is determined by the minimum of this curve and is reached at $B^*=3CD^2/(18C+E^2)$ and $\psi_0^*=C\psi_s^{*3}-B\psi_s^*$, with $\psi_s^*=DE/(18C+E^2)$. Modulated structures only exist inside the hysteresis cycle, which is delimited by $\psi_0=\pm(2/3)B\sqrt{B/3C}$ (dashed lines). The asymmetry of their domain of existence is a consequence of the nonlinear diffusion term, whose strength is fixed by the parameter E, and which breaks the inversion symmetry $\psi\leftrightarrow-\psi$. Figure 5, on the other hand, illustrates how the wave number and the velocity of the emerging non-Turing modulated structure depends on the input voltage ψ_0 for a fixed value of B.

Note that in Fig. 5, we plotted $k_r+\mathrm{Im}(\lambda)/V_{MF}$ instead of k_r in order to characterize the front oscillations. This is based on the flux of nodes across the front [12] but also follows directly from (8).

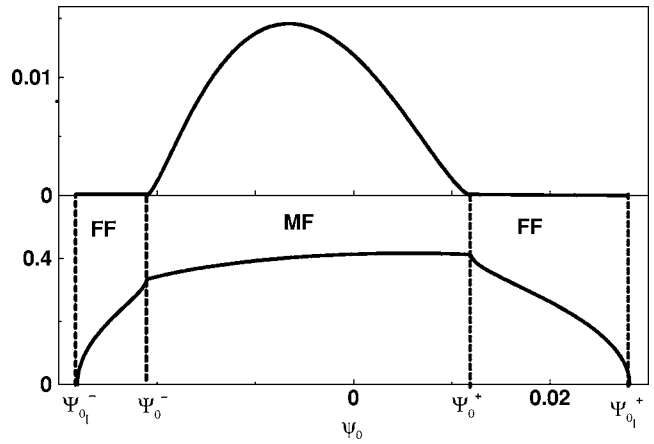

FIG. 5. The predicted wave number of flat (FF) and emerging non-Turing modulated (MF) structures and their velocities versus the input voltage ψ_0. The parameters and notations are the same as in Fig. 3 with $B=0.2$.

The transition is fully confirmed by the numerical simulations of Eq. (5), with localized Gaussian initial conditions (Fig. 3). At the first stage, the peak of the localized perturbation grows gradually in time until it reaches its maximum value (upper branch). This amplification process is accompanied by a propagation of the fronts into the region occupied by the unstable HSSs. Once flat fronts are established, small oscillations systematically start in the wings of the structures, as shown in Fig. 3 (second snapshot of the first line). These oscillations dominate the dynamics only asymptotically in time, according to the initial-value problem analysis. Finally, after a sufficiently long time, we observe that the whole domain can be covered by a textured solution that alternatively switches between upper and lower branches of the hysteresis cycle. This is consistent with the one-dimensional study in [12].

Equation (9) nicely emphasizes the roles of diffusion and bistability in the formation of modulated fronts. On the one hand, diffusion smoothes inhomogeneities and is therefore detrimental to the formation of fronts. On the other hand, the slope of ψ_s (ψ_0) gives the tendency for the system to jump as a whole towards either of the stable states of the hysteresis cycle. Hence it is no surprise that the maximum nonlinear diffusion $\mathcal{D}$ compatible with oscillations is directly given in terms of the slope $d\psi_0/d\psi_s=(d\psi_s/d\psi_0)^{-1}$, which is negative on the unstable branch. Intuitively, if the curve ψ_s (ψ_0) is nearly vertical, the system rapidly switches to either of the two stable states, leaving no time for oscillations to set in. Conversely, if the middle branch ψ_s (ψ_0) is nearly horizontal, the system hesitates for a longer time between the upper or the lower stable state, making front oscillations possible. In this case indeed, we have $|d\psi_s/d\psi_0| \ll 1$, i.e. $|d\psi_0/d\psi_s| \gg 1$ in Eq. (9). This simple criterion is illustrated in Fig. 3: all other things being equal, the fronts are modulated for the largest value of B, i.e., for the widest hysteresis cycle.

IV. BACK TO THE FULL MODEL

Let us now examine the transition from flat to modulated fronts in the original model. Specifically, we wish to draw the bifurcation diagram of Fig. 4 in the $(\phi_0, \alpha I_0)$ plane. To this end, we apply the method of steepest descent to the dispersion relation (3). Hence, as before, we look for the complex saddle point of $\Delta(k)$, which yields

$$V=\frac{\partial}{\partial k_i}\mathrm{Re}[\lambda(k_r,k_i)], \quad \frac{\partial}{\partial k_r}\{\mathrm{Re}[\lambda(k_r,k_i)]-k_iV\}=0,$$

and we impose that $\mathrm{Re}[\Delta(k_r,k_i)]$ vanishes. The resulting expressions are now much more complicated, but on the transition curve between flat and modulated fronts, $k_r=0$. This gives

$$V=k_i\left[2-a\mathcal{J}\cos\left(\frac{\phi}{2}\right)\cos\left(\frac{\phi}{2}+ak_i^2\right)\right],$$

$$0=-1+a\mathcal{J}\cos\left(\frac{\phi}{2}\right)\times\left[\frac{1}{2}\cos\left(\frac{\phi}{2}+ak_i^2\right)-ak_i^2\sin\left(\frac{\phi}{2}+ak_i^2\right)\right], \quad (14)$$

$$0=-1-k_i^2+\mathcal{J}\cos\left(\frac{\phi}{2}\right)\times\left[ak_i^2\cos\left(\frac{\phi}{2}+ak_i^2\right)-\frac{1}{2}\sin\left(\frac{\phi}{2}+ak_i^2\right)\right], \quad (15)$$

where $\mathcal{J}$ stands for

$$\mathcal{J}=\alpha I_0\exp[-\alpha I_{fb}/\varphi_{sat}]=\alpha I_0\exp[-\alpha I_0\cos^2(\phi/2)/\varphi_{sat}]. \quad (16)$$

Eliminating $\mathcal{J}$ between Eqs. (14) and (15), we obtain

$$\frac{a-ak_i^2}{2a^2k_i^2+2a^2k_i^4-1}=\tan\left(\frac{\phi}{2}+ak_i^2\right). \quad (17)$$

This last equation is easily solved:

$$\phi=\phi(k_i)=2\arctan\left(\frac{a-ak_i^2}{2a^2k_i^2+2a^2k_i^4-1}\right)-2ak_i^2.$$

Meanwhile, Eq. (14) yields

$$\mathcal{J}(k_i)=\frac{2\sec(\phi/2)}{a\cos(\phi/2+ak_i^2)-a^2k_i^2\sin(\phi/2+ak_i^2)}.$$

Hence, taking k_i as a parameter along the bifurcation curve between flat and modulated fronts, we have explicit formulas for $\phi(k_i)$ and $\mathcal{J}(k_i)$. For each value of k_i, we can thus solve (16) numerically and obtain $\alpha I_0(k_i)$. Finally, from (2), $\phi_0(k_i)=F(\phi(k_i),\alpha I_0(k_i),\pi/4)$.

The result is illustrated in Fig. 6 for a set of parameter values that are far from the conditions of nascent bistability. In particular, we take $a=0.51$, very different from a_c. The picture is essentially the same as in the simplified model, with ψ_0 and B replaced by ϕ_0 and αI_0, respectively. Although a modulational instability exists, its threshold is everywhere above $\alpha I_0 \approx 50$. Hence it has no influence at pumping intensities $\alpha I_0 \approx 5$.

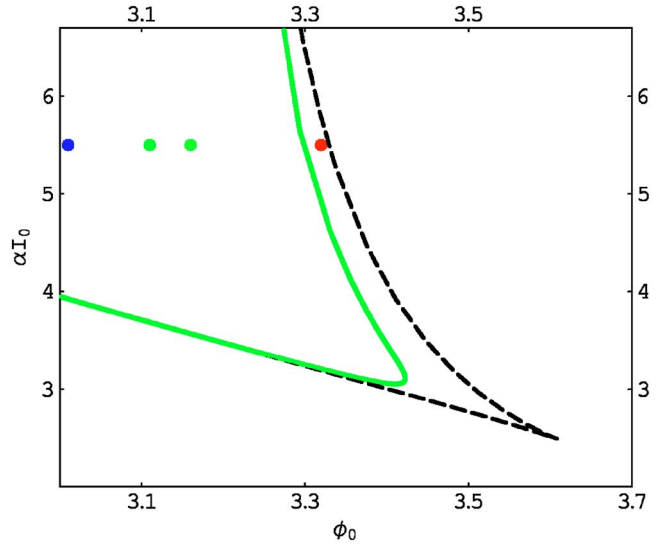

FIG. 6. (Color on line) Bifurcation diagram from flat to modulated fronts in the full model of the LCLV cavity. Dashed lines delimit the bistability domain. The region of existence of modulated fronts is the upper left part of the diagram enclosed by the full line. Parameter values, $\omega=3.14\times10^{15}$ s^{-1}, $L=1.335$ cm, $\ell=50$ μm, $\varphi=5$. This gives $a=0.51$.

The results of numerical simulations displayed in Figs 7–10 correspond to the four dots in Fig. 6, with $\alpha I_0=5.5$ and $\phi_0=3.32$, 3.16, 3.11, and 3.0, respectively. Figure 7 shows a flat front initiated by a Gaussian perturbation at the center of the domain. Initially, the system is on the unstable middle branch of the hysteresis cycle. The front invades the unstable domain from left to right. In the subsequent figures, modulated fronts are observed, in full agreement with the predictions. In Fig. 9, the front leaves behind a long-lived structure where domains in the upper stable state and in the lower stable state alternate. This is due to the fact that $\phi_0=3.11$ is close to the Maxwell point for switching fronts between the

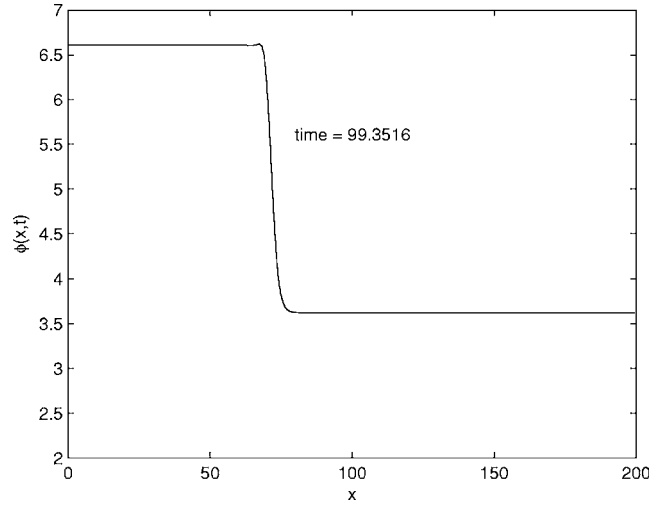

FIG. 7. Flat front in the full LCLV model. The front propagates from left to right. $a=0.51$, $\alpha I_0=5.5$, $\phi_0=3.32$. The initial condition is the unstable middle-branch solution plus a Gaussian perturbation $0.01\exp(-2x^2)$ centered at the origin.

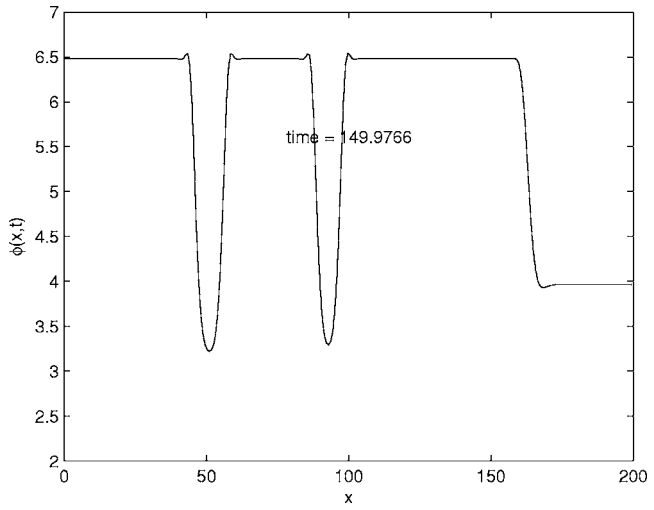

FIG. 8. Modulated front in the full LCLV model. $a=0.51$, $\alpha I_0=5.5$, $\phi_0=3.16$. The initial condition is the unstable middle-branch solution plus a Gaussian perturbation $0.01\exp(-2x^2)$. The final state long after the passage of the front is the upper stable state of the hysteresis cycle.

two *stable* states [3]. For $\phi_0=3.16$ (Fig. 8), these switching fronts move into the domain occupied by the lower branch, so that eventually, only the upper state remains. The reverse is true for $\phi=3.00$ as shown in Fig. 10.

V. SUMMARY

In summary, starting from the model describing the LCLV system with feedback, we have derived the modified Swift-Hohenberg equation in the nascent bistability limit. This allowed an in-depth analysis of the flat-modulated front transition. In particular, we found the particularly simple and physically meaningful formula (9) as a criterion for appear-

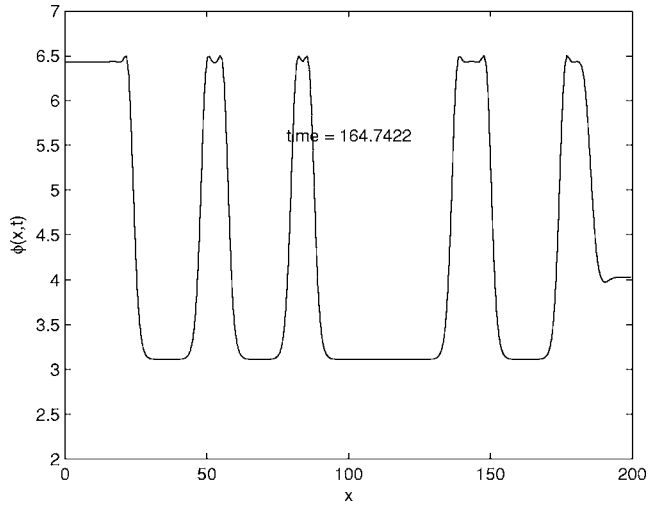

FIG. 9. Modulated front in the full LCLV model. $a=0.51$, $\alpha I_0=5.5$, $\phi_0=3.11$. The initial condition is the unstable middle-branch solution plus a Gaussian perturbation $0.01\exp(-2x^2)$. A long-lasting structure persists in the medium: the system is close to the Maxwell point for switching fronts between the two *stable* states.

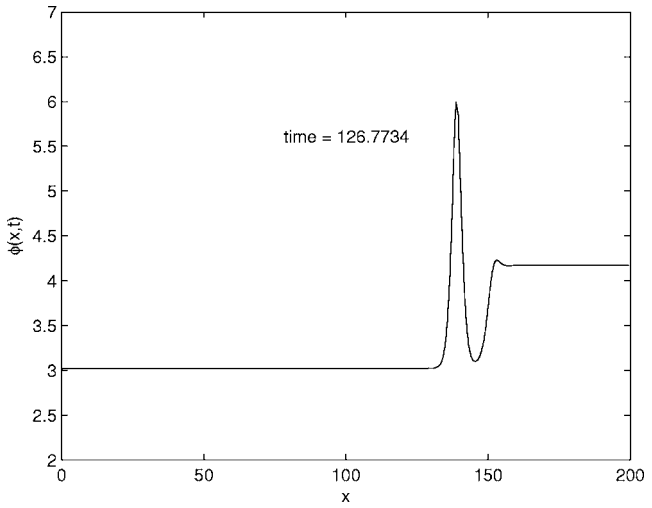

FIG. 10. Modulated front in the full LCLV model. $a=0.51$, $\alpha I_0=5.5$, $\phi_0=3.00$. The initial condition is the unstable middle-branch solution plus a Gaussian perturbation $0.01\exp(-2x^2)$. The final state is the lower stable state off the bistability cycle.

ance of modulations in the front, which involves the nonlinear damping of modulations [through $\mathcal{D}(\psi)$] and the propensity for the system to jump as a whole into a stable state (through $d\psi_0/d\psi_s$). A simple conclusion was that a wide bistability range is favorable to modulations. Clearly, from Fig. 6, this conclusion is valid in the full model too. In order for the modulated front to imprint a robust modulation in the system, it is necessary to be near the Maxwell point for the switching fronts between the upper and lower stable homogeneous steady states. At this point, these switching fronts are close to immobile.

We emphasize that the phenomenon exists in the absence of Turing (or modulational) instability and does not require any form of drift. Moreover it is not restricted to the limit of nascent bistability. This study constitutes the first step towards an experimental observation of non-Turing oscillations. The specific laboratory system considered, namely a LCLV with feedback, is promising because of the existence of many control parameters, and of its relatively slow (order of 1*s*) dynamics.

ACKNOWLEDGMENTS

We would like to thank W. van Saarloos, U. Ebert, P. Glorieux, R. Lefever, and E. Louvergneaux, for useful discussions. The Laboratoire de Physique des Lasers, Atomes et Molecules is Unité de Recherche Mixte du CNRS. The Centre d'Études et de Recherches Lasers et Applications is supported by the Ministère chargé de la Recherche, the Région Nord-Pas de Calais, and the Fonds Européen de Développement Économique des Régions. This research was supported in part by the Fonds National de la Recherche Scientifique (Belgium) and by the Interuniversity Attraction Pole program of the Belgian government. This work has also been partially supported by MIUR-FIRB Project No. RBNE01CW3M-001.

[1] M. C. Cross and P. C. Hohenberg, Rev. Mod. Phys. **65**, 851 (1993);J. D. Murray, *Mathematical Biology*, (Springer, Berlin, 1993).

[2] L. A. Lugiato, M. Brambilla, and A. Gatti, Adv. At., Mol., Opt. Phys. **40**, 229 (1998); W. Lange and T. Ackermann, J. Opt. B: Quantum Semiclassical Opt. **2**, 347 (2000); K. Staliunas and V. J. Sanchez-Morcillo, *Transverse Patterns in Nonlinear Optical Resonators*, (Springer-Verlag, Berlin, 2003); P. Mandel and M. Tlidi, J. Opt. B: Quantum Semiclassical Opt. **6**, R60 (2004); *Dissipative Solitons*, Lecture Notes in Physics Vol. 66, edited by N. Akhmediev and A. Ankiewicz (Springer, Berlin, 2005).

[3] N. N. Rosanov, in *Spatial Hysteresis and Optical Patterns* (Springer, Berlin, 2002).

[4] S. A Akhmanov, M. A. Vorontsov, and V. Yu. Ivanov, JETP Lett. **47**, 25 (1988); G. D'Alessandro and W. J. Firth, Phys. Rev. Lett. **66**, 2597 (1991).

[5] E. Pampaloni, P. L. Ramazza, S. Residori, and F. T. Arecchi, Phys. Rev. Lett. **74**, 258 (1995).

[6] E. Benkler, M. Kreuzer, R. Neubecker, and T. Tschudi, Phys. Rev. Lett. **84**, 879 (2000).

[7] A. Schreiber, B. Thuering, M. Kreuzer, and T. Tschudi, Opt. Commun. **136**, 415 (1997).

[8] P. L. Ramazza, U. Bortolozzo, and L. Pastur, J. Opt. A, Pure Appl. Opt. **6**, S266 (2004).

[9] E. Louvergneaux, C. Szwaj, G. Agez, P. Glorieux, and M. Taki, Phys. Rev. Lett. **92**, 043901 (2004).

[10] U. Bortolozzo, L. Pastur, P. L. Ramazza, M. Tlidi, and G. Kozyreff, Phys. Rev. Lett. **93**, 253901 (2004).

[11] L. A. Lugiato and R. Lefever, Phys. Rev. Lett. **58**, 2209 (1987).

[12] G. T. Dee and W. van Saarloos, Phys. Rev. Lett. **60**, 2641 (1988); W. van Saarloos, Phys. Rep. **286**, 29 (2003).

[13] N. N. Rosanov and G. V. Khodova, Opt. Spectrosc. **65**, 1399 (1988); N. N. Rosanov, in *Progress in Optics*, edited by E. Wolf (Elsevier, Amsterdam, 1996), Vol. 35.

[14] M. Santagiustina, P. Colet, M. San Miguel, and D. Walgraef, Opt. Lett. **23**, 1167 (1998); M. Taki, M. San Miguel, and M. Santagiustina, Phys. Rev. E **61**, 2133 (2000).

[15] R. Neubecker, G. L. Oppo, B. Thuering, and T. Tschudi, Phys. Rev. A **52**, 791 (1995).

[16] G. Kozyreff, S. J. Chapman, and M. Tlidi, Phys. Rev. E **68**, 015201(R) (2003); G. Kozyreff and M. Tlidi, *ibid.* **69**, 066202 (2004).

[17] P. Mandel, M. Georgiou, and T. Erneux, Phys. Rev. A **47**, 4277 (1993).

[18] S. Residori, A. Petrossian, T. Nagaya, and M. Clerc, J. Opt. B: Quantum Semiclassical Opt. **6**, S169 (2004); M. G. Clerc, A. Petrossian, and S. Residori, Phys. Rev. E **71**, 015205(R) (2005).

[19] R. J. Briggs, *Electron-Stream Interaction in Plasmas* (MIT Press, Cambridge, MA, 1964).

[20] L. Brevdo, J. Appl. Math. Phys. (ZAMP) **42**, 911 (1991).
[21] M. Santagiustina, P. Colet, M. San Miguel, and D. Walgraef, Phys. Rev. Lett. **79**, 3633 (1997); J. Opt. B: Quantum Semiclassical Opt. **1**, 191 (1999).
[22] H. Ward, M. Taki, and P. Glorieux, Opt. Lett. **27**, 348 (2003); H. Ward, M. N. Ouarzazi, M. Taki, and P. Glorieux, Phys. Rev. E **63**, 016604 (2000).
[23] C. M. Bender and S. A. Orszag, *Advanced Mathematical Methods for Scientists and Engineers* (Springer-Verlag, New York, 1999).